Characterization of EMI-(HF)$_{2.3}$F Using Carbon Xerogel Electrospray Thrusters

IEPC-2017-210

Catherine E. Miller[*], David Krejci[†] ,Caroline Bates[‡] ,Daniel Getty[§], and Paulo C. Lozano[¶]
Massachusetts Intitude of Technology, Cambridge, MA, 02139, USA

A fluorohydrogenated ionic liquid, EMI-(HF)$_{2.3}$F, was tested in a carbon xerogel based ion electrospray thruster. This ionic liquid has ten times the conductivity of what are considered high-conductivity ionic liquids (e.g., EMI-BF$_4$), making it an attractive option for increasing the thrust density of electrospray thrusters. As expected the emitted current was significantly higher than that of an EMI-BF$_4$ thruster, but it was not stable over time for any applied voltage. Additionally the positive mode was the least stable with very high levels of current interception on the extractor grid, whereas the negative mode operated in a more stable manner with less interception. Despite the lack of current stability, it was possible to characterize the emission using retarding potential analysis and time of flight mass spectrometry techniques. Significant levels of heavy ion cluster fragmentation were observed in addition to a small droplet population, which both served to reduce the specific impulse and efficiency. The results provide an indication of what the performance could be like, but are not sufficient to determine the long term operation performance. Future work is needed to understand the source of the current instability and to improve the thruster design so that long term firing is consistent and predictable.

Nomenclature

c_i	= ion velocity
c_{drop}	= drop velocity
e	= fundamental unit of charge
F	= thrust
f_0	= current fraction of monomers
f_{drop}	= droplet current fraction
f_f	= current fraction of fragmented dimers
f_i	= ion current fraction
I_{sp}	= specific impulse
I_0	= total source current
I_T	= total beam current
I_{TOF}	= time of flight curve
L	= flight length
$\dot{m}$	= total mass flow rate

[*]Graduate Research Assistant, Aeronautics and Astronautics, millerce@mit.edu
[†]Research Scientist, Aeronautics and Astronautics, krejci@mit.edu
[‡]Graduate Research Assistant, Aeronautics and Astronautics, clbates@mit.edu
[§]Graduate Research Assistant, Aeronautics and Astronautics, dgetty@mit.edu
[¶]Professor, Aeronautics and Astronautics, plozano@mit.edu

$$
\begin{aligned}
m_0 &= \text{mass of monomer ion} \\
m_1 &= \text{mass of dimer ion} \\
m_{drop} &= \text{mass of drop} \\
m_i &= \text{ion mass} \\
m_{pi} &= \text{mass of parent ion} \\
\eta_\epsilon &= \text{energy efficiency} \\
\eta_p &= \text{polydispersive efficiency} \\
q_i &= \text{ion charge} \\
t &= \text{time} \\
t_f &= \text{ion flight time} \\
t_{f,bi} &= \text{broken ion flight time} \\
V_0 &= \text{applied potential} \\
V_{br} &= \text{acceleration potential at which the ion cluster breaks} \\
\xi &= \text{mass ratio of dimer to monomer}
\end{aligned}
$$

I.   Introduction

ION electrospray thrusters have the potential to revolutionize the capabilities of CubeSats and microsatellites. They are power-efficient, compact, modular systems that can be used for both main propulsion and attitude control. Currently, CubeSats have limited propulsion options[1]. This is namely due to the challenge of miniaturizing propulsion technologies, such as ion engines and Hall thrusters, while maintaining nominal lifetimes and efficiencies[2]. Another challenge is the restriction placed on secondary payloads which prevent many CubeSats from carrying pressurized gas tanks, a critical component for many propulsion systems. Ion electrospray thrusters have a significant advantage in that they are naturally suited to small scale applications, have the potential for high efficiency and long lifetimes, and do not require pressurized gas tanks. Thus ion electrospray thrusters could provide CubeSats with the propulsive capabilities needed to complete long term missions as well as those requiring precision attitude control.

Ion electrospray thrusters are based on ionic liquid ion sources (ILIS), which are ion beams produced from ionic liquids. Room temperature molten salts, called ionic liquids, are composed of purely positive and negative molecular, and sometimes atomic, ions. Strong electric fields can be used to evaporate ions directly from the liquid, resulting in an ion beam that can be accelerated with kilovolt electric potentials. An ion electrospray thruster consists of an array of ILIS beams, in effort to attain thrust levels useful for CubeSat applications. These thrusters, called the ion Electrospray Propulsion System (iEPS), have been under development in the Space Propulsion Lab at the Massachusetts Institute of Technology since 2011. Much research effort has gone into understanding the physics of ionic liquid ion sources in addition to manufacturing techniques[3], material selection[4,5], and performance characterization[6–8]. The iEPS thrusters have undergone many design improvements and have been demonstrated to operate with good performance, although not as high as theoretically possible.

In addition to improving thruster lifetime and efficiency[9], a major area of interest is increasing the thrust density. This of course can be achieved through the densification of emitters. This approach is limited by the properties of the thruster materials as well as the capabilities of available micromachining techniques. If the thrust level is to be increased without changing the thruster architecture, the propellant properties must be modified. This can be achieved through increasing the temperature of a given propellant, which serves to increase the electrical conductivity of the fluid and thus the ion evaporation rates. Alternatively, an ionic liquid with high electrical conductivity at room temperatures can be selected. Many ionic liquids used in electrospray thrusters have electrical conductivities on the order of ~ 1 Si/m, but there are some liquids that have conductivities an order of magnitude higher. One of these liquids, EMI-$(HF)_{2.3}F$, is the subject of investigation in this work. Such a high conductivity liquid could potentially provide higher thrust densities while operating in the pure ionic regime, allowing for high specific impulse as well. A liquid like this is of great interest for ion electrospray thrusters, thus the focus of this paper is to provide an initial characterization of the performance of EMI-$(HF)_{2.3}F$.

II. Ion Electrospray Propulsion Physics

Ion electrospray thrusters are based on ionic liquid ion sources. An ionic liquid ion source can use many different architectures such as externally wetted[10], internally wetted[7], and capillary emitters[11]. A schematic of an externally wetted emitter is shown in Fig. 1. An electrochemically etched, chemically roughened
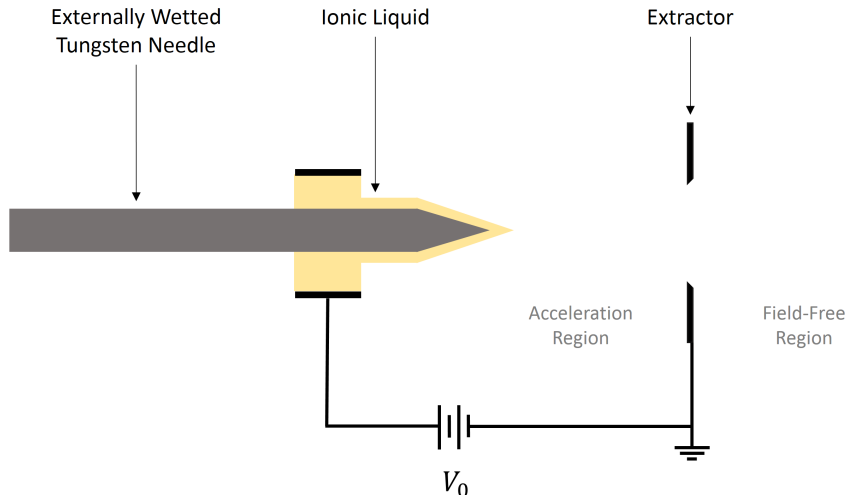
Figure 1. Schematic of an ionic liquid ion source.[12]

tungsten needle with a tip radius of curvature on the order of 15 microns is used as the emitter in Fig. 1. Ionic liquid coats the surface of the needle and is held in a reservoir away from the tip. The needle is placed less than a millimeter from a metal extractor plate with an aperture. Approximately 1-2 kilovolts can be applied between the ionic liquid reservoir and the extractor to produce a beam of individual ions and ion clusters. These sources can be operated using both positive and negative potentials to produce positive and negative ion beams, respectively.

The ionic species in the beam depend on the composition of the ionic liquid propellant, which consists purely of positive and negative ions. For example, one of the most well-characterized ionic liquids in ion electrospray thrusters is $EMI\text{-}BF_4$. A positive ion beam emanating from an $EMI\text{-}BF_4$ ILIS typically consists of $\sim 50\%$ EMI^+ "monomers" and $\sim 50\%$ $(EMI\text{-}BF_4)\text{-}EMI^+$ "dimers"[10]. Monomers refers to single ions whereas dimers refers to the type of ion cluster that consists of a single ion attached to a cation-anion pair, also called a neutral. Other ionic liquids may produce larger ion clusters such as trimers, tetramers, and pentamers which are single ions attached to two, three, and four neutrals respectively. These ion clusters are metastable and may break apart midflight. This occurs because the clusters are imparted with excess energy during the evaporation process and the Coulombic attraction between the molecular ions may not be strong enough to hold the cluster together for long. This process is referred to as fragmentation, and it has been experimentally shown that different ionic liquids show different amounts of cluster break up[13,14]. At this time, it is not well understood how the ionic liquid properties and ion molecular structure affects the composition and amount of fragmentation in ILIS beams.

The presence and fragmentation of ion clusters in ILIS beams has a significant effect on propulsive performance. Ion clusters of varying sizes have different masses but the same electric charge, so when accelerated through the same electric potential, they leave the thruster at different speeds. When ion clusters break apart while being accelerated, the ion fragments leave the thruster at speeds according to the local value of the electric potential where the fragmentation event occurred. Since clusters can break apart anywhere within the thruster, they will leave the thruster at a spread in final velocities. This further increases the polydisperity of the ion beam, which is a term used to quantify the level to which ions leave the thruster at varying speeds. The most propulsively efficient configuration is to have all ions exiting the

thruster with the same mass and same speed[13]. When the ion beam is polydisperse, the propulsive efficiency decreases.

Consider an ion beam consisting of only monomers and dimers. The polydispersive efficiency can be described using the following equation:

$$\eta_p = \frac{\left(1 + (\sqrt{\xi} - 1)f_0 + \frac{1}{3}f_f\left(2\sqrt{\xi}\frac{1-\sqrt{\xi}}{1-\xi} - 1\right)\right)^2}{1 + (\xi - 1)f_0} \tag{1}$$

where $\xi = m_1/m_0$, f_0 is the current fraction of monomers, and f_f is the current fraction of broken ions resulting from dimer fragmentation[13]. This formula was derived assuming that fragmentation of dimers occurs uniformly with respect to the acceleration potential. Fig. 2 shows the effect of beam composition and fragmentation on: (a) the propulsive efficiency, and (b) the thrust and specific impulse. The beam

(a)

(b)
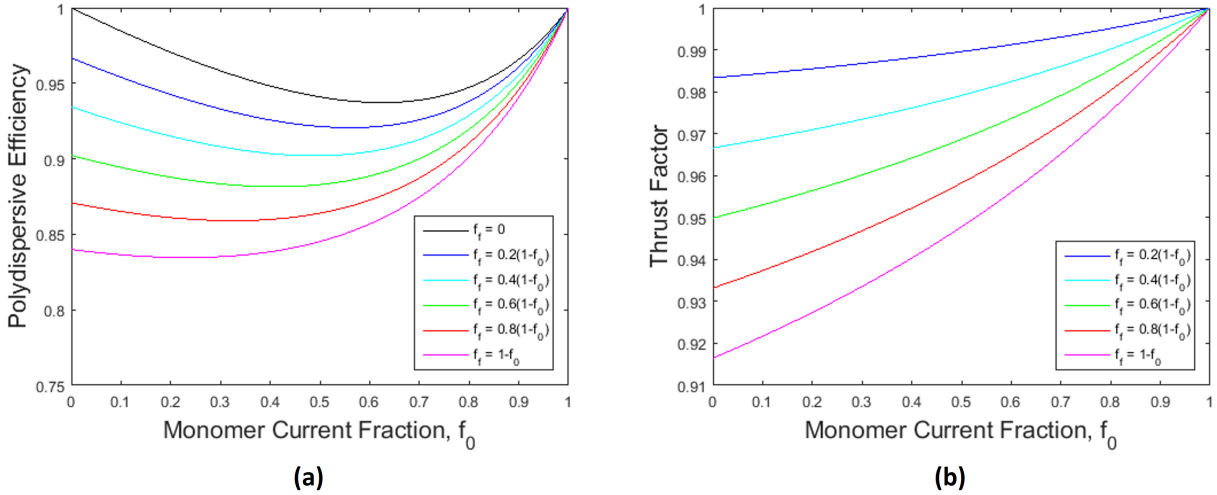
Figure 2. Effect of polydisperity on (a) propulsive efficiency, and (b) specific impulse and thrust.

composition has an important effect on the propulsive performance. Ideally the beam would consist of only one type of ion, but this is not the case in reality. Instead ionic liquid propellants must be chosen based on how propulsively favorable their ILIS beam compositions are. Since there is not a theoretical understanding of how ionic liquid composition controls the beam composition, one must experimentally measure it for each liquid. The same can be said for fragmentation of ion clusters, which has a significant effect on performance. There is not a good way to predict what percentage of ion clusters will break apart in an ILIS beam produced using an untested liquid. Therefore the beam composition and amount of fragmentation must be measured in the lab, and then the effect on propulsive efficiency can be computed.

III.   Ion Source Design

THE ionic liquid EMI-(HF)$_{2.3}$F has exceptional properties that make it an attractive propellant for ion electrospray thrusters. This liquid was developed in Japan by Prof. Hagiwara[15]. Table 1 displays the properties of EMI-(HF)$_{2.3}$F and EMI-BF$_4$ for comparison.   EMI-(HF)$_{2.3}$F has a very high electrical conductivity, which should allow for higher ion evaporation rates, emission currents, and thrust per emitter than EMI-BF$_4$[16]. The thrust density of an EMI-BF$_4$ ion electrospray thruster is $\sim$ 0.5 N/m^2 [7], so EMI-(HF)$_{2.3}$F could potentially reach 5 N/m^2, which is better than most ion engines. Most other liquid properties are very similar to that of EMI-BF$_4$, which indicates that the source should operate at similar voltages in the pure ionic regime. EMI-(HF)$_{2.3}$F has one major undesirable property in that it holds some degree of acidity that in time will react with silicates. This means that the current design of ion electrospray thruster arrays, which uses porous glass emitters, cannot be used to test EMI-(HF)$_{2.3}$F since the liquid etches away

Table 1. Ionic Liquid Properties [10,15]

Property	EMI-$(HF)_{2.3}$F	EMI-BF_4
Conductivity (Si/m)	10	1.4
Surface Tension (dyn/cm)	48	45.2
Density (g/cm^3)	1.13	1.28
Viscosity (mPa s)	4.9	37
Electrochemical Window (V)	3.1	4.3
Cation	EMI$^+$	EMI$^+$
Cation Mass (amu)	111.2	111.2
Anion	$(HF)_2F^-$; $(HF)_3F^-$	BF_4^-
Anion Mass (amu)	59; 79	86.8

the sharpness of the emitter tips over short periods of time.

The new emitter arrays used in these experiments were made from a porous resorcinol formaldehyde carbon aerogel. The process required resorcinol, deionized water, formaldehyde, and acetic acid. First, 3 g of deionized water was added to 2.46 g of resorcinol, and the resorcinol completely dissolved in the water. While the resorcinol was dissolving, the beaker containing the mixture was covered in parafilm to prevent evaporation. Next, 4.3g of 37% formaldehyde was added to the solution, followed by 0.088 g of acetic acid. The solution was poured into a mold and the mold placed in a sealed container. The container then sat in a fumehood for 18 hours. Then the container was heated in an oven at 40°C for 6 hours. The oven temperature was then increased to 60° C for 18 hours. Finally, the oven temperature was increased to 80° C for 30 hours. After the xerogel arrays had solidified in the oven, they were pyrolized in a 900°C furnace with an argon flow rate of 400 sccm. Finally, the xerogel arrays were annealed in the furnace to remove any remaining impurities, and leaving behind only carbon. The furnace was initially heated to 110°C with no argon flow. Then the temperature was increased to 295°C, with an argon flow rate of 20 sccm. Lastly, the temperature was raised to 430°C and the argon flow rate was increased to 100 sccm. Once the xerogel arrays had been annealed, the emitter tips were created using laser ablation.[17]

Full emitter arrays patterned with 480 tips on 1 cm^2 carbon chips were prepared. Fig. 3 shows an image of a carbon xerogel thruster loaded with the fluorohydrogenated ionic liquid propellant. Full emitter arrays
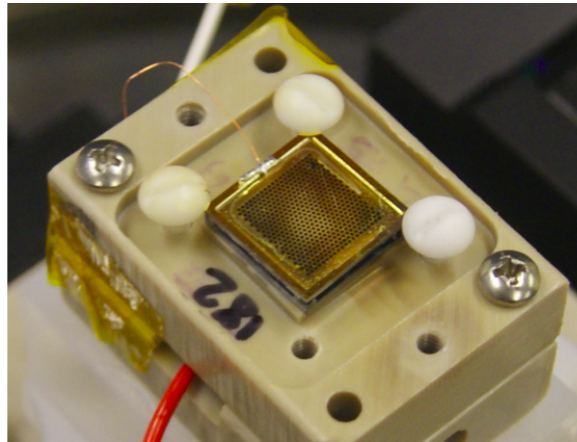
Figure 3. Ion electrospray thruster loaded with EMI-$(HF)_{2.3}$F on a temporary mount.

were modified for time of flight testing since the detector can be saturated by the high current levels produced by 480 tips. Instead, only 5-10 tips are needed to attain time of flight data. The array was examined under the microscope to select the area of the array that has the best tips and most uniform surface under the tips. Next, most of the tips were removed using a razor and a platinum wire hook. Once only the desired

tips remained, the final step was to gently spray the array with nitrogen gas to remove any debris from the tip removal process.

The full and partial emitter arrays consist of a carbon xerogel emitter secured to a silicon frame with epoxy. The extractor was carefully aligned so that each tip was nearly in the center of the extractor holes. The extractor was secured to the emitter by the white teflon screws shown in Fig. 3. The propellant was loaded on the back of the chip. EMI-$(HF)_{2.3}$F is potentially hygroscopic, so care was taken to minimize the time between loading propellant and placing the thruster in vacuum. Once several drops of liquid absorbed into the array, a thin layer of paper cloth was placed over the exposed part of the bottom of the array. Then a stainless steel spring was placed in contact with the paper soaked with liquid. A screw was used to make the electrical connection between the high voltage wire and the stainless steel spring inside the thruster mount. In the case of the partial emitter array experiments, the spring was later substituted with a carbon electrode in attempt to mitigate electrochemical reactions.

The carbon electrode was made using a similar process as that used to make the emitter array. First, a mold was prepared. The mold had cavities to create 64 electrodes. At the bottom of each cavity was a small hole, slightly larger than 0.010" in diameter. For each cavity, a piece of platinum wire 0.010" in diameter and approximately 8 mm long was threaded through the small hole and bent into a small loop on the inside of the cavity. Most of the length of the wire remained on outside bottom of the mold. The hole was then covered with silicone sealant and the sealant allowed to cure for 24 hours. The resorcinol formaldehyde solution for the electrode was similar to that of the array, but used 19.68 g of resorcinol, 24 g of water, 28.64 g of formaldehyde, and 0.70 g of acetic acid. The solution was then fed into each of the cavities in the mold using a syringe. Next, the mold was placed in a sealed container and placed in the fumehood for 24 hours. After 24 hours, the container was placed in the oven for 24 hours at 40°C. Next, the oven temperature was increased to 60°C for 24 hours, and then to 80°C for 48 hours. The container was then removed from the oven and allowed to sit open in the fumehood for 24 hours. Lastly, the open container was placed back in the 80°C oven for another 48 hours. Once the mold had cooled, the electrodes were removed from the mold, then pyrolized and annealed using the same processes as those used for the array. Finally, the electrodes were shaped. The electrode used in this experiment was shaped to a diameter of 4.7 mm and height of approximately 3 mm using a dremel and sandpaper. First, the electrode was rolled over sandpaper to remove the shiny outer layers. Next, a dremel was used to cut the electrode from 11 mm in length to 4 mm in length. Then the top of the electrode was sanded until it was flat and the length of the electrode was 3 mm. Finally, the electrode was placed in an isopropanol bath for 30 minutes followed by a 30 acetone bath to remove any particles created by the sanding.

IV.   Experimental Methods

THE experimental goal for this work is to determine the propulsive performance of EMI-$(HF)_{2.3}$F in ion electrospray thrusters. The quantities of interest are of course the specific impulse, thrust, and efficiency. One relatively straightforward method to estimate these parameters is time of flight mass spectrometry (TOF). Time of flight measurements reveal the composition of the ion beam as well as the percentage of ion clusters that fragment in the acceleration region. This information can be used to estimate the propulsive performance, the details of which are presented in the next section. To measure the thrust and specific impulse with greater certainty, a thrust balance is required. By measuring the thrust as a function of time and massing the thruster before and after the experiment, one can compute the specific impulse. For the purpose of this work, time of flight measurements are sufficient to estimate the propulsive performance. Additionally the TOF technique provides a wealth of information that can be used to better understand the ion evaporation and fragmentation physics of ionic liquid ion sources.

Time of flight mass spectrometry works by relating the flight times of ions to their masses. Fig. 4 shows a schematic of the TOF detector used in this work. The instrument consists of an electrostatic deflection gate, used to interrupt the ion beam, and a current collector, in this case a Channeltron electron multiplier[14]. When the gate is activated, the beam is deflected so that no current is measured by the collector. When the gate is inactive, the beam can travel freely to the collector. As the gate is switched from inactive to active, the TOF mass spectrum is measured. The flight length of the detector used in this work is ~ 81 cm. The detector has an acceptance angle of less than $1°$, so it only samples a very small portion of the ion beam. This removes the effects of beam spreading to allow for high resolution measurements at the expense of being unable to measure the properties of the full ion beam.
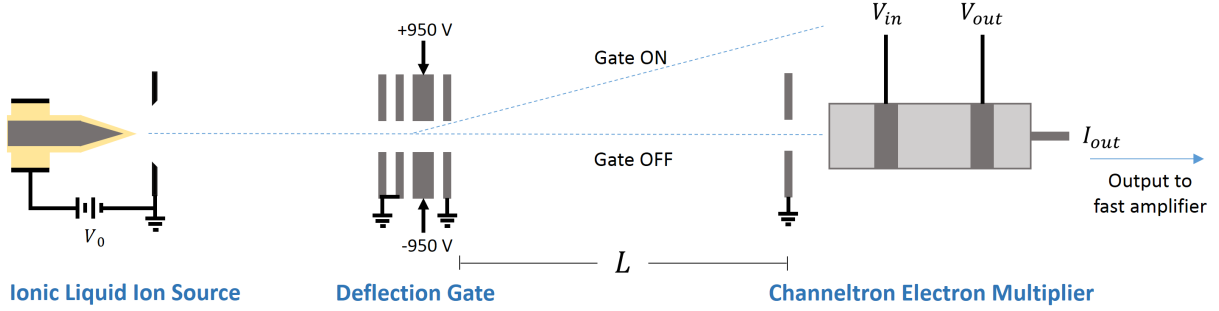
Figure 4. Schematic of time of flight mass spectrometer.

Ions and ion clusters of varying masses that are extracted by the same electric potential, V_0, will exit the thruster at different speeds. Thus they will be collected by the time of flight detector at different times given by the following equation:

$$t_f = L\sqrt{\frac{m_i}{2q_i V_0}} \qquad (2)$$

where t_f is the flight time, L is the flight distance, m_i is the mass of the ion, q_i is the charge of the ion, and V_0 is the potential through which the ion is accelerated[14]. This equation applies only to ions and ion clusters that have not fragmented within the thruster. With sufficient time resolution, the percentage of ion clusters of a given type that break up within the acceleration region can be measured. When ion clusters break apart within the thruster, they are accelerated to velocities corresponding to the local value of the electric potential where the fragmentation event occurred. Since these ions can break apart anywhere in the acceleration region, they are accelerated to a spread in final velocities and thus a spread in flight times. The flight time for a broken ion is given by the following equation:

$$t_{f,bi} = \frac{L}{\sqrt{\frac{2q_i V_0}{m_i}\left(1 - \frac{V_{br}}{V_0}\left(1 - \frac{m_i}{m_{pi}}\right)\right)}} \qquad (3)$$

where $t_{f,bi}$ is the flight time of a broken ion, V_{br} is the electric potential at which the fragmentation event occurred, and m_{pi} is the mass of the parent ion[14]. Ions that break up outside of the thruster reach the detector at the same time an unbroken ion cluster would, since their velocity is not modified, so the TOF measurements are sensitive only to fragmentation within the acceleration region.

Idealized TOF measurements are shown in Fig. 5 for ion beams with and without fragmentation. It is assumed that these ion beams consist only of monomers and dimers. In Fig. 5(a) the collected current is zero until about 15 microseconds, which is the time that the fastest ions, the monomers, arrive at the detector. After their arrival, the current level remains flat until about 30 microseconds after the gate switched, which is when the heavier, slower dimers arrive at the detector. Thus by measuring the relative fractions of the two types of ions, the beam composition can be determined. In Fig. 5(b), 50% of the dimers fragment into a monomer plus a neutral within the thruster. This is assumed to occur uniformly with respect to the acceleration potential, meaning there is no preferred potential for break up to occur. The broken ion, which has the mass of a monomer, is accelerated to velocities always faster than the dimers that survive the acceleration region but always slower than the monomers that are evaporated from the tip. If the time resolution is sensitive enough, it may be possible to determine the distribution of fragmentation with respect to the acceleration potential and verify if it is uniform or not.

The TOF curves in Fig. 5 are highly idealized. In reality, the TOF detector has a limited bandwidth and as such it has a non-zero response time. The detector used in this work has a response time of a few hundred nanoseconds, which is very good and allows detailed characterization of the beam composition and fragmentation. There is also noise in the measurement, which further complicates determining the beam
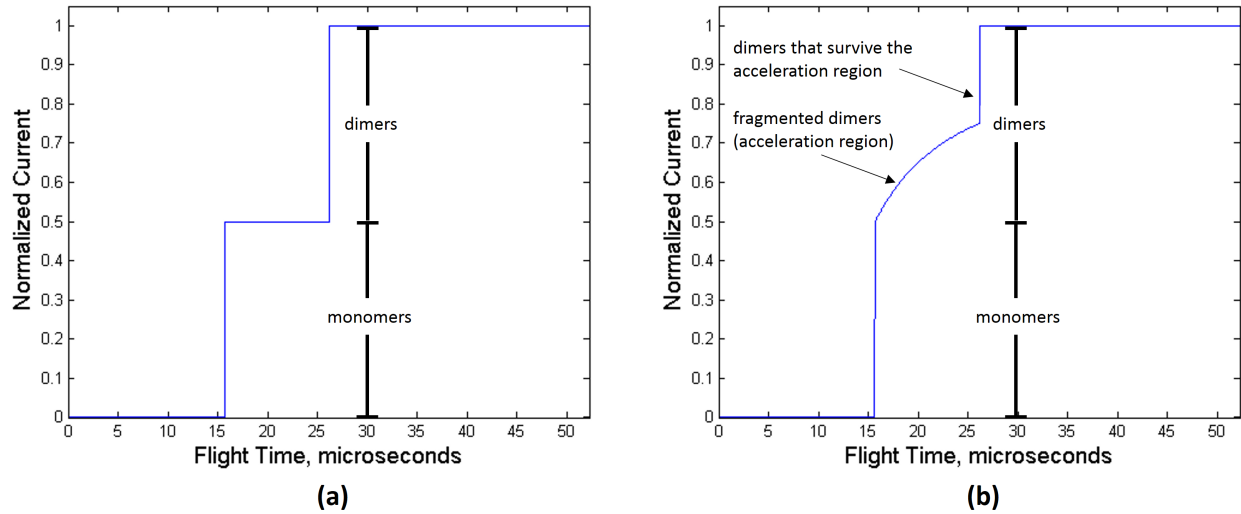
Figure 5. Idealized TOF curves for (a) beam without fragmentation, (b) beam with fragmentation.

composition. As long as the source is firing in a stable manner, the noise sources are typically just thermal noise and ringing from the operation of the electrostatic gate. The ringing noise settles out before the lightest ions arrive in most cases, so this does not pose much of an issue. The thermal noise blurs the TOF curves, which necessitates averaging hundreds of TOF scans in order to obtain a cleaner measurement. Thus this TOF detector is operated such that many TOF curves are averaged together, while the thruster operates at a stable current level, resulting in TOF curves that are suitable for estimating the thruster performance.

In addition to time of flight mass spectrometry, retarding potential analysis (RPA) is a very useful tool to measure the energy distribution of the ion beam. The energy distribution allows for a more detailed study of the fragmentation characteristics, which is of interest for characterizing the performance of an ionic liquid. Fig. 6 shows a schematic of a planar RPA. A retarding potential analyzer consists of several semi-
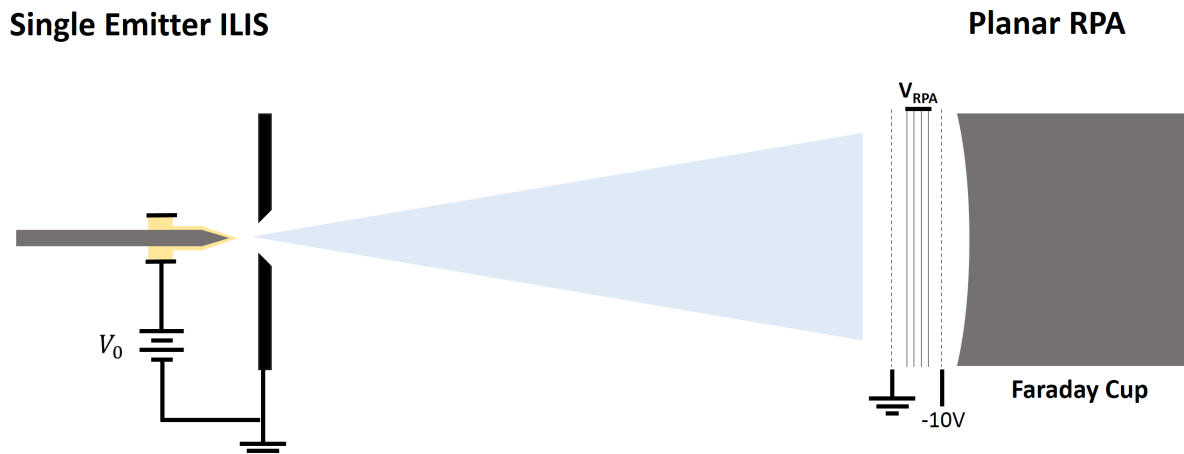
Figure 6. Schematic of a planar RPA.[12]

transparent metallic grids placed in front of a current collecting surface. The first grid is grounded to ensure

that the potential between the source and detector is flat and is at ground potential. The next set of grids are the retarding grids, which are biased from ground to at least the source potential. As the retarding potential is increased, the ions are slowed down and stopped, preventing them from being collected by the detector. The last grid is typically biased to at least - 10 V to prevent secondary electrons created by ion impacts on the current collecting surface from escaping the detector. To measure the energy distribution, the collected current is measured as a function of the retarding potential. Ideally, the energy distribution of the ion beam would be monoenergetic, with an energy corresponding to the source potential, as shown in Fig. 7(a). However in reality, the energy distribution of ILIS beams is distributed between a monoenergetic
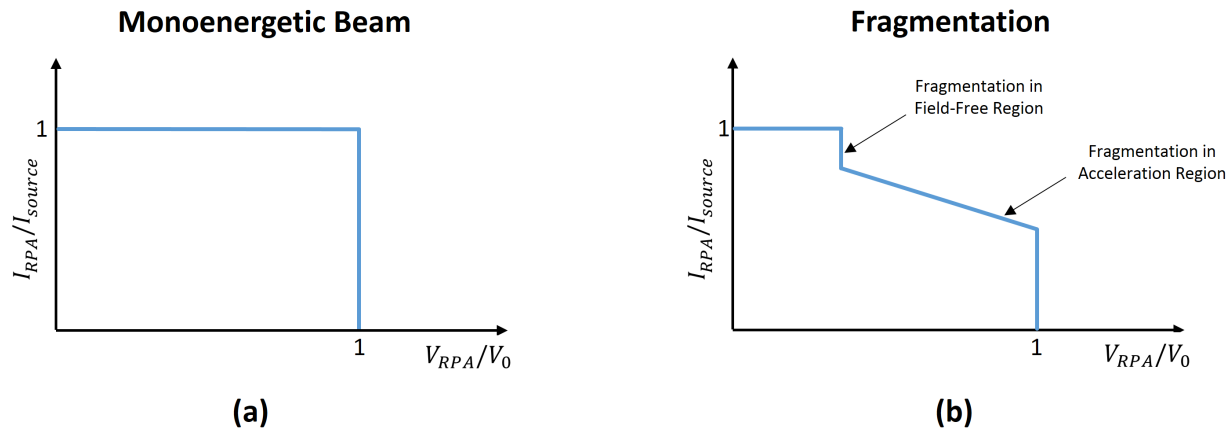
Figure 7. Idealized RPA curves for: (a) monoenergetic ion beam, and (b) ion beam with fragmentation.[12]

ion population and low energy ions produced by fragmentation. An idealized energy distribution for an ion beam with clusters that break apart both in the acceleration and in the field-free region outside the source could look something like that in Fig. 7 (b). Analyzing the lower energy features in the RPA data allows for the determination of how much fragmentation occurs in each region, among other things which have been detailed elsewhere[12]. The RPA used in this work has planar stainless steel grids and a Faraday cup collector. It has a 0.25" aperture and was placed 50 cm from the source.

V.   Data Analysis

MANY analysis steps are required to extract useful data from the raw TOF curves. First a calibration curve, taken when the source is turned off, is subtracted from the raw TOF curve. This removes some of the ringing signature as well as any non-zero offset from the amplifier. Then the data can be binned according to flight time in effort to further smooth out the TOF curve. At this point, the steps corresponding to unfragmented ions and ion clusters can be identified based on their flight times. Using the relative current fractions, the beam composition, including the fraction of ion clusters that fragment within the acceleration region, can be determined. The regions in the TOF curve where fragmentation is present require more attention to detail. One could assume that the fragmentation occurs uniformly with respect to the acceleration potential and use formulas similar to the one presented in previous sections. However this may not be the best path to take, especially considering that there is usually a non-negligible fraction of highly solvated ion fragments which would make the derivation of analytical formulas particularly challenging. Instead it is more efficient and more accurate to compute the efficiency, specific impulse, and thrust using numerical methods.

For each species, both the momentum fraction and mass fraction must be computed from the TOF curve. For monoenergetic species, this is as easy as reading the step height and flight time off the curve. The momentum fraction, $f_i m_i c_i$, is given by:

$$f_i m_i c_i = f_i m_i \frac{L}{t_{f,i}} \tag{4}$$

where f_i is the current fraction of that particular type of ion, m_i is the mass of the ion, and $t_{f,i}$ is the flight time of the ion. The mass fraction is simply just $f_i m_i$. For fragmented species, the derivative of the TOF curve needs to be integrated over. The momentum fraction for a particular type of fragmented ion is:

$$f_i m_i c_i = m_i \int \frac{dI_{TOF}}{dt} \left(\frac{L}{t} \right) dt \tag{5}$$

where $\frac{dI_{TOF}}{dt}$ is the derivative of the normalized time of flight curve and t is the flight time. The range over which the integral is performed corresponds to the flight times when fragmented ions of a particular type arrive at the detector. For example to account for dimers that break into monomers, one would integrate between the monomer flight time and the dimer flight time, since this is the range of times that the broken dimers reach the detector. The mass fraction of broken ions can be computed in the same way as the monoenergetic ions.

To account for droplets, the mass distribution is assumed to follow:

$$m_{drop} = \eta_\epsilon \frac{2eV_0}{(L/t)^2} \tag{6}$$

where e is the elementary unit of charge and η_ϵ is the energy efficiency, assumed to be 90% in this work. The mass fraction of droplets can be computed using the following expression:

$$f_{drop} m_{drop} = \int \frac{dI_{TOF}}{dt} m_{drop} dt \tag{7}$$

and the momentum fraction of droplets can be found using:

$$f_{drop} m_{drop} c_{drop} = \int \frac{dI_{TOF}}{dt} m_{drop} \left(\frac{L}{t} \right) dt \tag{8}$$

The case of droplets is not particularly different from the case of ions. The major difference is that the mass of the droplets varies as a function of flight time, and the energies are typically lower than the ion energies.

To estimate the thrust, the following expression is used:

$$F = I_B \sum_i f_i \frac{m_i}{q_i} c_i \tag{9}$$

where F is the thrust. This is simply a summation of the mass fractions of each species multiplied by the total particle flow rate, which is the current divided by a ion charge. The specific impulse can be computed using the following equation:

$$I_{sp} = \frac{\sum_i f_i m_i c_i}{g \sum_i f_i m_i} \tag{10}$$

where I_{sp} is the specific impulse and g is the acceleration due to gravity. The specific impulse is simply the ratio of the sum of the momentum flow rate and the sum of the mass flow rate, scaled by $1/g$. Finally, the polydispersive efficiency can be computed as follows:

$$\eta_p = \frac{F^2/2\dot{m}}{I_0 V_0} = \frac{\left(\sum_i f_i \frac{m_i}{q_i} c_i \right)^2}{2V_0 \sum_i f_i \frac{m_i}{q_i}} \tag{11}$$

VI. Full Thruster Array Results and Discussion

A full thruster array was fired in a 16" diameter, 30" long vacuum system with a 685 l/s turbo pump. The current-voltage relationship is shown in Fig. 8(a). The emitted current levels are much higher than those for an EMI-BF$_4$ thruster[7]. The emission was observed to be quite unstable in comparison to other ionic liquids such as EMI-BF$_4$. The intercepted current was also observed to be much higher than what is considered acceptable performance for ion electrospray thrusters. Fig. 8(a) highlights the asymmetry between positive and negative mode operation. The thruster was not shorted and yet had 100% interception
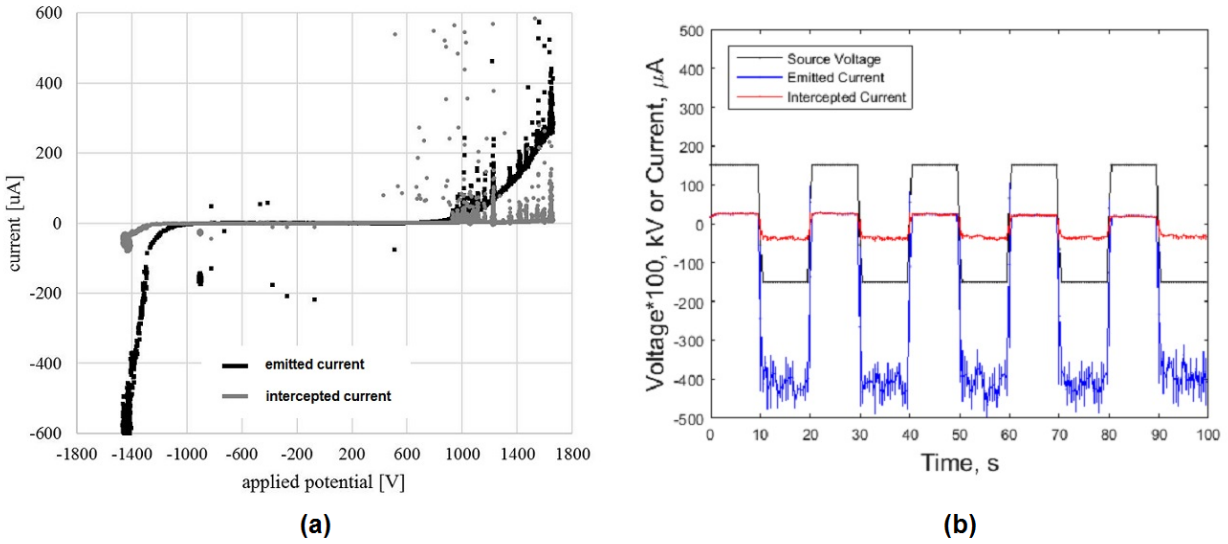
Figure 8. EMI-(HF)$_{2.3}$F full thruster array firing data.

in the positive mode while having less than 10% interception in the negative mode. This is shown in Fig. 8(b) when the thruster was fired using a constant voltage square wave. This sort of behavior is highly unusual for ion electrospray sources.

In another test of a carbon emitter array with EMI-(HF)$_{2.3}$F, the emission was more symmetric. The emitted current and intercepted current for a square voltage wave are shown in Fig. 9. The emitted current is
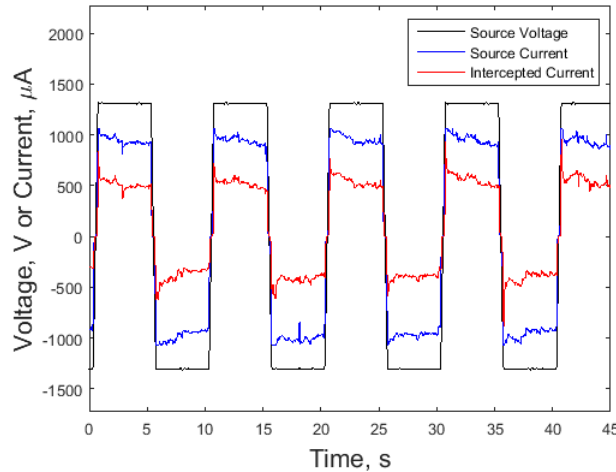
Figure 9. EMI-(HF)$_{2.3}$F full thruster array with symmetric emission.

remarkably high, nearly 1 mA. This is ten times the emitted current of an EMI-BF$_4$ thruster. The symmetry observed in Fig. 9 was not observed in any other tests.

The beam divergence was measured using the RPA Faraday cup mounted on a rotating arm within the chamber. The results are shown in Fig. 10. The beam divergence distribution is very non-uniform, which is likely due to fluctuations in the source current levels as a function of time. The beam divergence angle is approximately 60°, which is comparable to EMI-BF$_4$ thruster[7]. By assuming the distribution is roughly parabolic, which is not unreasonable in the case of -613μA, the angular efficiency can be estimated using a method outlined in work by Lozano and Martinez-Sanchez[18]. The estimated angular efficiency is 80%, and the estimated thrust reduction factor due to the angular spread is 0.89.
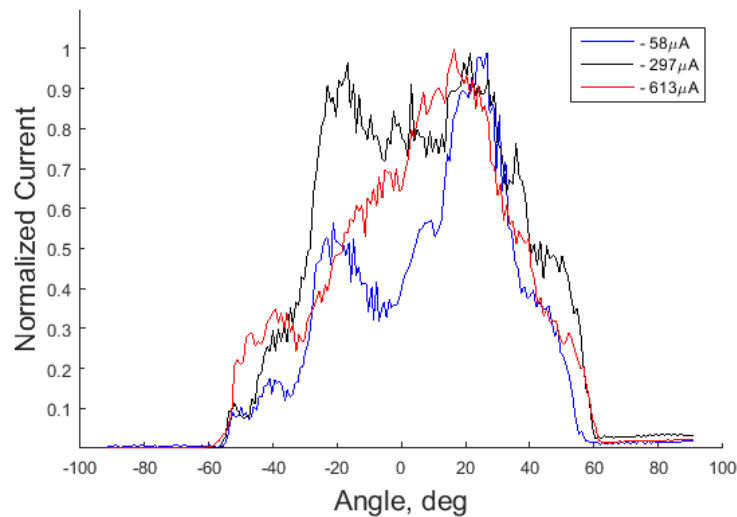
Figure 10. EMI-(HF)$_{2.3}$F full thruster array divergence.

Retarding potential analysis measurements were made using a Faraday cup with a 0.25" aperture placed 50 cm from the source. Many RPA scans were made at a constant voltage and were averaged together in attempt to smooth out the source noise. Fig. 11 shows the results for various current levels in the negative mode. The current level was not stable over the time period of data acquisition, so it is difficult to gain much
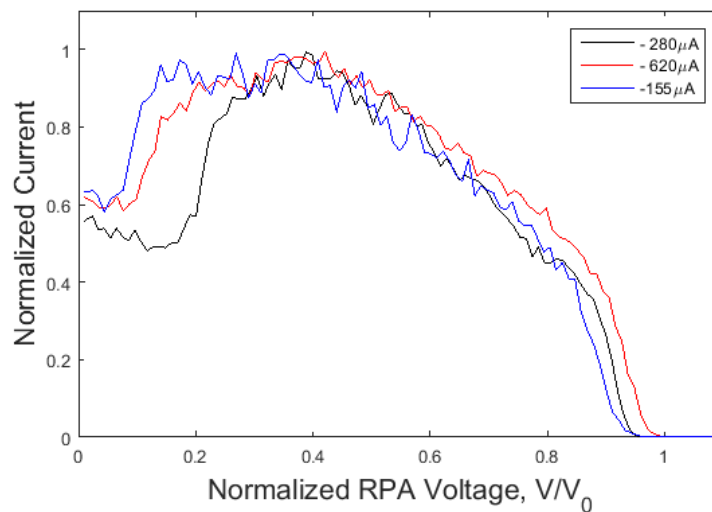
Figure 11. EMI-(HF)$_{2.3}$F full thruster array retarding potential analysis measurements.

insight from these RPA curves. There appears to be significant fragmentation in the acceleration region and perhaps a lower energy droplet population. It also appears that $\sim 40\%$ of the beam is monoenergetic. There does not appear to be any features that would indicate that there is fragmentation in field free space, which may be a result of source instability and not a reflection of the true beam characteristics. There is also a large feature at low retarding voltages where the collected current drops significantly from the maximum. While RPA features similar to this have been observed in the past, which have been attributed to secondary electron currents, a feature as strong as this has not been observed. It is unclear if the source of this feature is a result of secondary electrons, source instability, or something else.

After firing, the thruster was disassembled. The stainless steel spring used to apply the high voltage to the thruster array was black. This indicates that a chemical or electrochemical reaction of some kind had occurred during the course of testing. It is quite possible that the reactions that caused the stainless steel

spring to turn black are also related to the source instability and asymmetric behavior. In positive mode operation, the HF-rich negative ions accumulate on the counter electrode. This could result in reactions that form iron fluoride, a compound with poor electrical conductivity. Additionally hydrogen gas would be evolved, which would leave through the emitter pores, contributing to the source instability.

VII.   Partial Thruster Array Results and Discussion

PARTIAL thruster arrays were fired in a 10" diameter, 30" long vacuum system with a 430 l/s turbo pump. The TOF detector is mounted in a $\sim$ 16" flight tube attached to the back end of the chamber. The thruster fired in the negative mode, but positive emission could not be achieved even when voltages in excess of 3 kV were applied. The thruster was not shorted and still had liquid between the high voltage wire and the thruster array, indicating a good electrical connection. Since the electronics for the time of flight detector only allow for positive ion detection, TOF data was not obtained for the negative mode.

It was concluded that electrochemistry may have played a role in preventing emission in the positive mode, especially considering the effects observed with the full thruster array. To reduce the effects of electrochemical reactions, a high contact area distal contact electrode was fabricated to replace the stainless steel spring that connected the high voltage to the thruster array. The distal contact electrode consists of a small cylinder of carbon xerogel with a platinum wire inside, which should be less reactive than the stainless steel. The high voltage is applied to the platinum wire, which is then transmitted to the ionic liquid in the thruster through the ionic liquid impregnated in the electrode. The benefits of using a distal contact electrode are well studied[9]. In summary, a distal contact allows for thruster operation in a single polarity for longer durations and prevents electrochemical reactions from occurring at the tips of the emitters, reducing degradation. The electrochemical reactions are distributed throughout the high area carbon electrode, rather than being concentrated on the small contact area of the stainless steel spring.

A thruster with a more compatible distal electrode was able to achieve emission in the positive mode, albeit with high interception current. Even with the distal contact, it appears that electrochemical effects of some kind may have affected the stability of emission. Despite this, it was possible to measure the current-voltage relationship by ramping the voltage slowly over time. A triangular wave was used with a period of 200 s. The wave peaks were adjusted such that the positive mode reached a higher peak voltage than the negative mode. This was chosen because the negative mode fires readily at lower voltages and the current increases dramatically at higher voltages. Fig. 12(a) shows the current-voltage relationship for both positive and negative modes taken for a single scan. This scan was taken after firing for approximately 45 minutes.

(a)

(b)
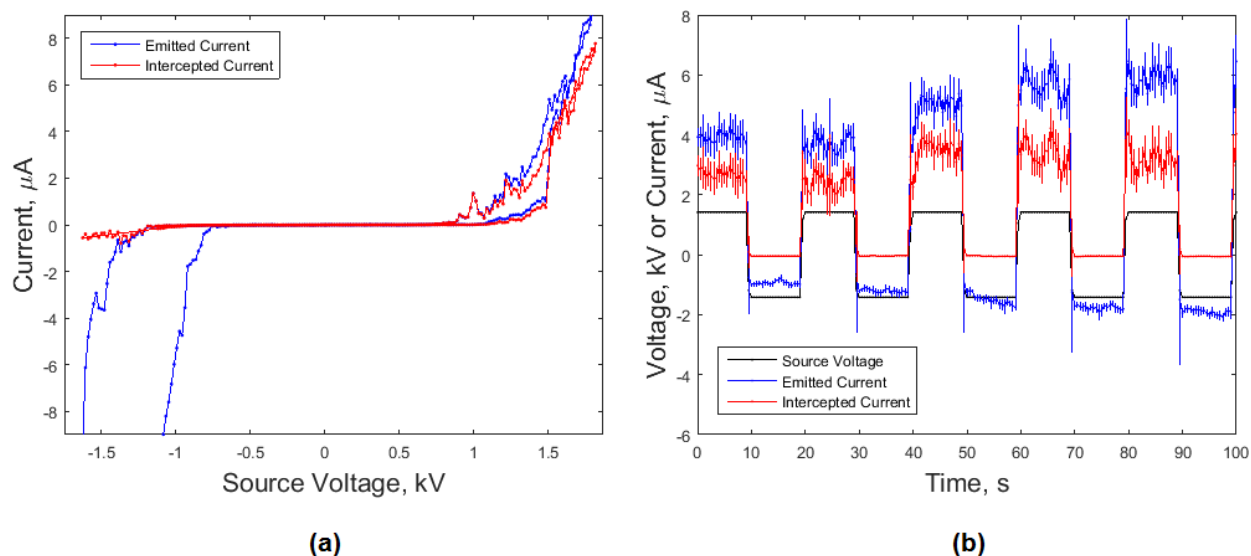
Figure 12.   EMI-(HF)$_{2.3}$F partial array firing data.

At this point the interception in the positive mode had increased significantly from what was observed during the TOF data collection period. The emission is highly asymmetric, something that is not usually seen to

this degree with other ionic liquids. The negative mode operated with much lower interception and appeared to be somewhat more stable as shown in Fig. 12(b).

Time of flight measurements were taken when the source was firing in the positive mode. While plenty of signal was measured at the detector, it was still challenging to make these measurements since the emitted current levels were not stable over even short periods of time. The TOF measurements reported in this work are a snapshot of how the source behaves under various conditions. They do not represent the beam characteristics over long periods of time since the TOF curves fluctuated significantly while measurements were taken. The time of flight measurements in Fig. 13 show that the source produced mainly ions, although in some cases a significant droplet population was observed. This is remarkable considering the high flow rates. The beam consists of monomers, dimers, broken heavy ion clusters, and some droplets. The monomer
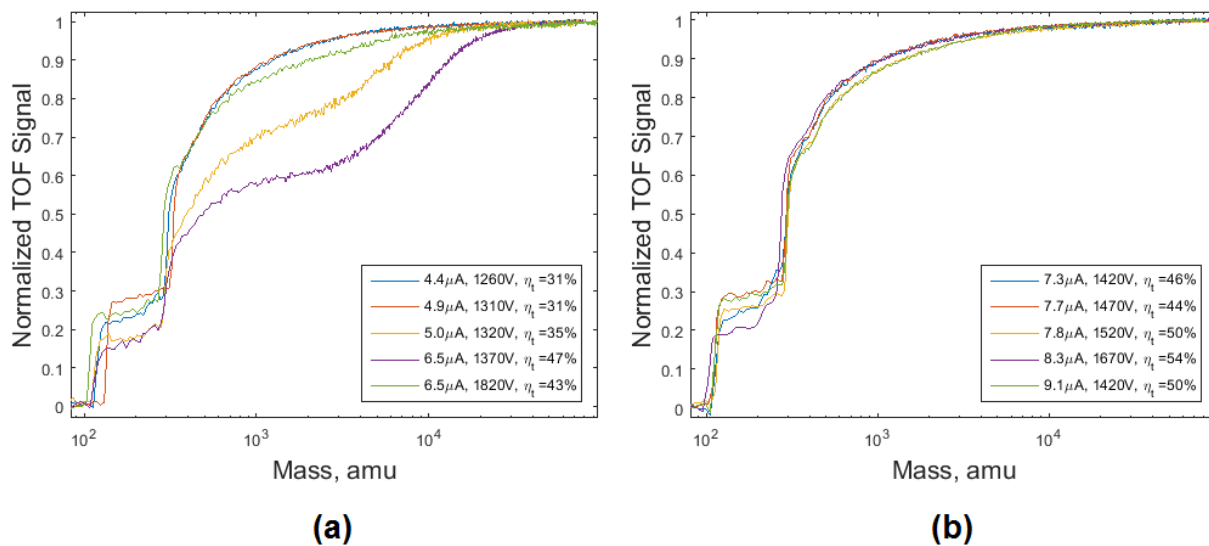
Figure 13. EMI-(HF)$_{2.3}$F TOF data. Legend displays the source current, voltage, and transmission efficiency.

is EMI$^+$ with a mass of 111 amu. The dimer step corresponds to (EMI-(HF)$_2$F)EMI$^+$, which has a mass of 281 amu. The dimer corresponding to (EMI-(HF)$_3$F)EMI$^+$, which has a mass of 301 amu, was not observed. The TOF curves show no stable trimers and instead indicate fragmentation of heavy ion clusters within the acceleration region. At some point these heavy ion clusters transistion to very small droplets with masses on the order of 10^3-10^5 amu.

Despite the lack of source stability, the beam composition can still be used to get an idea of how the source performs in terms of thrust, efficiency, and specific impulse. The TOF curve was divided into various regions for the computation, the details of which are outlined in section V. The size of the steps corresponding to monomers and dimers that survive the acceleration region can be read from the TOF curves directly. This was done computationally by binning the step, fitting the step with a smoothing spline, taking the second derivative, and finding points of inflection which indicate the times where the step begins and ends. The regions corresponding to fragmentation of ion clusters were binned, fitted using a smoothing spline, and integrated over according to the equations in section V. It was assumed that the ion clusters derive from the (HF)$_2$F$^-$ anion, which is supported by the TOF observations. The maximum size ion cluster was assumed to be (EMI-(HF)$_2$F)$_{10}$EMI$^+$. Any remaining part of the TOF curve was assumed to derive from droplets with energies corresponding to 90% of the acceleration potential. This assumption is not supported by any measurements using this ion source, although it is not unreasonable considering that it is well known that droplets have lower energies than the acceleration potential. The beam composition is shown in Table 2 and the estimated performance is shown in Table 3 for various set points. The current fraction of monomers in the beam is denoted by f_0, dimers that survive the acceleration region by $f_{1,m}$, dimers that break up in the acceleration region by $f_{1,f}$, heavy ion clusters that break up in the acceleration region by f_f, and droplets by f_{drops}. The transmission efficiency, which is the ratio of the current that leaves the thruster to the total thruster current, is denoted by η_t. The polydispersive efficiency is denoted by η_p. The thrust to power ratio

Table 2. Beam Composition

Current, μA	Voltage, kV	f_0	$f_{1,m}$	$f_{1,f}$	f_f	f_{drop}
4.4	1.26	19%	26%	9%	38%	8%
4.9	1.31	25%	29%	5%	34%	7%
5.0	1.32	17%	20%	4%	33%	25%
6.5	1.37	14%	14%	7%	25%	41%
6.5	1.82	24%	30%	4%	31%	11%
7.3	1.42	22%	25%	15%	31%	7%
7.7	1.47	28%	32%	4%	29%	7%
7.8	1.52	24%	33%	5%	30%	9%
8.3	1.67	18%	34%	10%	30%	7%
9.1	1.42	28%	28%	5%	31%	9%

is shown in the final column of Table 3.

Table 3. Performance Characteristics

Current, μA	Voltage, kV	η_t	I_{sp}, s	η_p	Thrust, μN	Thrust/$I_0 V_0$ μN/W
4.4	1.26	31%	1230	54%	0.49	89
4.9	1.31	31%	1230	51%	0.54	84
5.0	1.32	35%	840	52%	0.83	125
6.5	1.37	47%	590	51%	1.58	178
6.5	1.82	43%	1010	41%	0.98	83
7.3	1.42	46%	1030	43%	0.87	85
7.7	1.47	44%	1310	52%	0.91	81
7.8	1.52	50%	920	39%	1.04	87
8.3	1.67	54%	1280	48%	1.06	77
9.1	1.42	50%	1210	50%	1.1	85

Several observations can be made using the TOF curves and performance estimates. The monomer population is fairly low, ranging from 14%-18%, while the fraction of all dimers is relatively high, ranging from 21%-44%. The percent of dimers that break up within the acceleration region ranges from 11-38%. The percentage of the beam corresponding to heavy ion clusters that fragment within the acceleration region is significant, ranging from 25%-38%. The droplet population is approximately 7%-9% for beams that appear to consist of mostly ions. When the beam transitions to a mixed ion-droplet mode, the droplet population is as high as 41%. the effect of droplets and ion cluster fragmentation on performance is significant. The specific impulse and polydispersive efficiency suffer as a result. The cases with the highest droplet populations show the lowest specific impulse, highest thrust, and highest thrust to power ratio, which is to be expected. Note that the performance characteristics are not corrected for the beam divergence. The estimated thrust for a full emitter array operating in the ion regime is on the order of 70-80 μN, which is $\sim$ 6 times higher than the typical thrust achieved using EMI-BF$_4$[7]. These observations should not be used to make strong conclusions about the performance of the source since they only represent a snapshot during unstable operation.

VIII.   Conclusion

THE ionic liquid EMI-$(HF)_{2.3}$F was successfully fired using carbon xerogel emitter arrays in ion electrospray thrusters. The observed emission characteristics, namely the asymmetry between positive negative modes and current level instability, were unexpected and are not typical of other ionic liquids used in ion electrospray thrusters. Results from firing full and partial emitter arrays support the notion that electrochemical reactions of some form may be responsible for the unusual emission characteristics. Additionally, the very low viscosity of the liquid may play a role in the emission instability. The surface tension should be re-measured to confirm that it is comparable to that of EMI-BF$_4$. It is possible that with low surface tension and low viscosity, the liquid could be more readily pulled out the sides of the emitters, resulting in off-axis emission and high interception. This is an area of recommended future study since little is understood about the specific physical phenomena that occurs. Through a better understanding of this phenomena, design changes could be made so that the electrochemical, chemical, and other unwanted effects are mitigated. This is a necessary step before EMI-$(HF)_{2.3}$F should be used in spaceflight. Alternatively, sulfonium-based hydrofluorogenated ionic liquids have higher viscosity and may be more suitable for this application.

The performance characteristics of EMI-$(HF)_{2.3}$F were measured using RPA and TOF techniques. The RPA measurements using the full thruster array show significant amounts of fragmentation within the acceleration region. Additionally the beam divergence angle is $\sim 60°$, which is not unusual for EMI-BF$_4$ thrusters using porous glass emitter arrays. The TOF measurements show that the beam typically consists of mostly ions; however there is significant fragmentation within the acceleration region and a small droplet population. These characteristics result in lower specific impulse and propulsive efficiency than desired. The estimated thrust is quite high, approximately 6 times higher than EMI-BF$_4$ thrusters, which was expected due to the high electrical conductivity of EMI-$(HF)_{2.3}$F. Once the thruster is designed in such a way that stable emission can be achieved, the performance of the liquid should be re-evaluated. The measurements detailed in this work only provide a snapshot of what the performance could be like and should not be used to predict long term thruster performance. With future work, it is possible that a EMI-$(HF)_{2.3}$F ion electrospray thruster could produce significantly higher thrust than EMI-BF$_4$ thrusters while maintaining a comparable specific impulse.

Acknowledgments

References

[1] Poghosyan, A., & Golkar, A., "CubeSat evolution: Analyzing CubeSat capabilities for conducting science missions," *Progress in Aerospace Sciences*, Vol. 88, 2017, pp. 59-83.

[2] Khayms, V., "Advanced propulsion for microsatellites," Ph.D. Dissertation, Aeronautics and Astronautics Dept., Massachusetts Institute of Technology, Cambridge, MA, 2000.

[3] Courtney, D., "Ionic liquid ion source emitter arrays fabricated on bulk porous substrates for spacecraft propulsion," Ph.D. Dissertation, Aeronautics and Astronautics Dept., Massachusetts Institute of Technology, Cambridge, MA, 2011.

[4] Coffman, C., Perna, L., Li, H, & Lozano, P., "On the manufacturing and emission characteristics of a novel borosilicate electrospray source," *49th AIAA/ASME/SAE/ASEE Joint Propulsion Conference*, July 14-17, 2013, San Jose, CA.

[5] Perez-Martinez, C., "Engineering ionic liquid ion sources for ion beam applications," Ph.D. Dissertation, Aeronautics and Astronautics Dept., Massachusetts Institute of Technology, Cambridge, MA, 2016.

[6] Mier-Hick, F., "Spacecraft charging and attitude control characterization of electrospray thrusters on a magnetically levitated testbed," Ph.D. Dissertation, Aeronautics and Astronautics Dept., Massachusetts Institute of Technology, Cambridge, MA, 2017.

[7] Krejci, D., Mier-Hicks, F., Thomas, R., Haag, T., & Lozano, P., "Emission characteristics of passively fed electrospray microthrusters with propellant reservoirs," *Journal of Spacecraft and Rockets*, Vol. 52, No. 2, 2017, pp. 447-458.

[8] Guerra-Garcia, C., Krejci, D., & Lozano, P., "Spatial uniformity of the current emitted by an array of passively fed electrospray porous emitters," *Journal Of Physics D: Applied Physics*, Vol. 49, No. 11, 2016.

[9] Brikner, N., "On the identification and mitigation of life-limiting mechanisms of ionic liquid ion sources envisaged for propulsion of microspacecraft," Ph.D. Dissertation, Aeronautics and Astronautics Dept., Massachusetts Institute of Technology, Cambridge, MA, 2015.

[10] Lozano, P., and Martinez-Sanchez, M., "Ionic Liquid Ion Sources: Characterization of Externally Wetted Emitters," *Journal of Colloid and Interface Science*, Vol. 282, No. 2, 2005, pp. 415-421.

[11] Romero-Sanz, I., Bocanegra, R., Fernàndez de la Mora, J. F., & Gamero-Castaño, M., "Source of heavy molecular ions

based on Taylor cones of ionic liquids operating in the pure ion evaporation regime," *Journal Of Applied Physics*, Vol. 94, No. 5, 2003, 3599-3605.

[12]Miller, C., & Lozano, P., "Measurement of the fragmentation rates of solvated ions in ion electrospray thrusters," *52nd AIAA/ASME/SAE/ASEE Joint Propulsion Conference*, July 25-27, 2016, Salt Lake City, UT.

[13]Coles, T., & Lozano, P., "Investigating efficiency losses from solvated ion fragmentation in electrospray thruster beams," *49th AIAA/ASME/SAE/ASEE Joint Propulsion Conference*, July 14-17, 2013, San Jose, CA.

[14]Miller, C., "On the stability of complex ions in ionic liquid Ion sources," Master's Thesis, Aeronautics and Astronautics Dept., Massachusetts Institute of Technology, Cambridge, MA, 2015.

[15]Hagiwara, R., Hirashige T., Tsuda T., & Ito, Y., "A highly conductive room temperature molten fluoride: EMIF2.3HF," *Journal of the Electrochemical Society*, Vol. 149, No. 1, 2002, pp. D1-D6.

[16]Lozano, P., Wardle, B., Moloney, P., & Rawal, S., "Nanoengineered thrusters for the next giant leap in space exploration," *Materials Research Society MRS Bulletin*, Vol. 40, No. 10, 2015, pp. 842-849.

[17]Rojas-Herrera, J. & Lozano, P., "Mitigation of anomalous expansion of carbon xerogels and controllability of mean-pore-size by changes in mold geometry," *Journal of Non-Crystalline Solids*, Vol. 458, 2017, pp. 22-27.

[18]Lozano, P., & Martínez-Sánchez, M., "Efficiency estimation of EMI-BF4 ionic liquid electrospray thrusters," *41st AIAA/ASME/SAE/ASEE Joint Propulsion Conference & Exhibit*, July 10-13, 2005, Tuscon, AZ.